

Modification of valence-band symmetry and Auger threshold energy in biaxially compressed $\text{InAs}_{1-x}\text{Sb}_x$

S. R. Kurtz, R. M. Biefeld, and L. R. Dawson

Sandia National Laboratories, Albuquerque, New Mexico 87185

(Received 1 August 1994)

Strained-layer superlattices (SLS's) with biaxially compressed $\text{InAs}_{1-x}\text{Sb}_x$ were characterized using magnetophotoluminescence and compared with unstrained $\text{InAs}_{1-x}\text{Sb}_x$ alloys. Holes in the SLS exhibited a decrease in effective mass, approaching that of the electrons. In the two-dimensional limit, a large increase in the Auger threshold energy accompanies this strain-induced change in SLS valence-band symmetry. Correspondingly, the activation energy for nonradiative recombination in the SLS's displayed a marked increase compared with that of the unstrained alloys. Strained-layer superlattices and alloy activation energies are in agreement with estimated Auger threshold energies.

Frequently, the Auger-1 process (i.e., an electron and hole recombine by scattering a second electron up into the conduction band) dominates radiative recombination in narrow band-gap III-V semiconductors, and as a result, the wavelength of diode lasers operating at room temperature has been limited to $\leq 2.1\text{--}2.3\ \mu\text{m}$.¹ In a biaxially compressed III-V layer, the $|3/2, \pm 3/2\rangle$ hole ground state can increase the in-plane, electron-hole effective mass ratio (m_e^*/m_h^*) over that found in bulk material. In the two-dimensional limit, this effective-mass ratio will result in an increased threshold energy for Auger-1.²⁻⁴ Therefore, midwave infrared ($2\text{--}6\ \mu\text{m}$) emitters with biaxially compressed active regions may exhibit improved performance and higher-temperature operation. Emitters with heterostructures incorporating compressively strained $\text{InAs}_{1-x}\text{Sb}_x$ active regions have recently been demonstrated.^{5,6} In this paper, we will describe the optical characterization of $\text{InAs}_{1-x}\text{Sb}_x$ strained-layer superlattices (SLS's) and present evidence indicating that a large increase in Auger-1 threshold energy results from the valence-band symmetry of the biaxially compressed layer.

$\text{InAs}_{1-x}\text{Sb}_x$ alloys and SLS's were grown by metal-organic chemical-vapor deposition (MOCVD) on InAs substrates. The MOCVD sources were trimethylindium, trimethylantimony, trimethylgallium, and arsine. Samples were grown at a temperature of $475\ ^\circ\text{C}$, at a pressure of 625 torr, and using a V/III ratio of approximately 10.⁵ Strained-layer superlattices and ternary compositions, layer thicknesses, and lattice constants were determined from both (004) and (115) or (335) x-ray rocking curves.⁷ Throughout our studies of As-rich, $\text{InAs}_{1-x}\text{Sb}_x$ (5–50% Sb), the band gaps of our InAsSb alloys were smaller than accepted values.⁸ This $\text{InAs}_{1-x}\text{Sb}_x$ band-gap anomaly was observed in both MOCVD and molecular-beam-epitaxy-(MBE-) grown samples. Electron-diffraction results indicate compositional ordering and phase separation may occur in the As-rich $\text{InAs}_{1-x}\text{Sb}_x$ grown at low temperatures by vapor phase epitaxy.⁹ As demonstrated

in the following discussion, the $\text{InAs}_{1-x}\text{Sb}_x$ material displays single phase, random-alloy-like optical properties except for the band-gap anomaly, and we assume that the strain imposed by the InAs heterostructure dominates any internal strain occurring with domains of the $\text{InAs}_{1-x}\text{Sb}_x$. Hall measurements and p - n junction studies show that the MOCVD grown, $\text{InAs}_{1-x}\text{Sb}_x$ material is n type.⁵ The samples had background carrier concentrations in the range $1\text{--}5 \times 10^{16}\ \text{cm}^{-3}$.

Midwave infrared photoluminescence was measured by operating a Fourier transform infrared (FTIR) spectrometer in a double-modulation mode.⁵ In the magnetophotoluminescence experiments, a fluoride optical fiber was used to transmit infrared light in the magnet cryostat. The photoluminescent light was collected by the fiber and analyzed with the FTIR equipped with an InSb photodiode. All measurements were made in the Faraday configuration with the magnetic field parallel to the growth (001), direction of the sample. All experiments were performed at the low optical pump power with a Nd:YAG (yttrium aluminum garnet) laser. Photoluminescence energy and line shape were independent of pump power, and photoluminescence intensity was proportional to optical pump power, assuring that the sample remained extrinsic, with negligible change in the majority carrier concentration during illumination.

Interband, magnetophotoluminescence measurements were used to confirm $\text{InAs}_{1-x}\text{Sb}_x$ SLS valence-band symmetry and to estimate effective masses. In Fig. 1, spectra for an $\text{InAs}_{0.91}\text{Sb}_{0.09}/\text{In}_{0.87}\text{Ga}_{0.13}\text{As}$ SLS (90-Å/130-Å layer thicknesses) are compared with those for unstrained $\text{InAs}_{0.93}\text{Sb}_{0.07}$ and InAs alloys. Photoluminescence spectra for the SLS and alloys [Figs. 1(a) and 1(b)] consist of a single peak in the $3\text{--}4\text{-}\mu\text{m}$ range, with linewidth ≤ 10 meV. Excitonic behavior is observed at low magnetic fields; in all samples the photoluminescence peak energy is insensitive to magnetic field for $B < 2T$, characteristic of a diamagnetic exciton. [See Fig. 1(c).] Also, the $\text{InAs}_{1-x}\text{Sb}_x$ and InAs alloy spectra display a field-

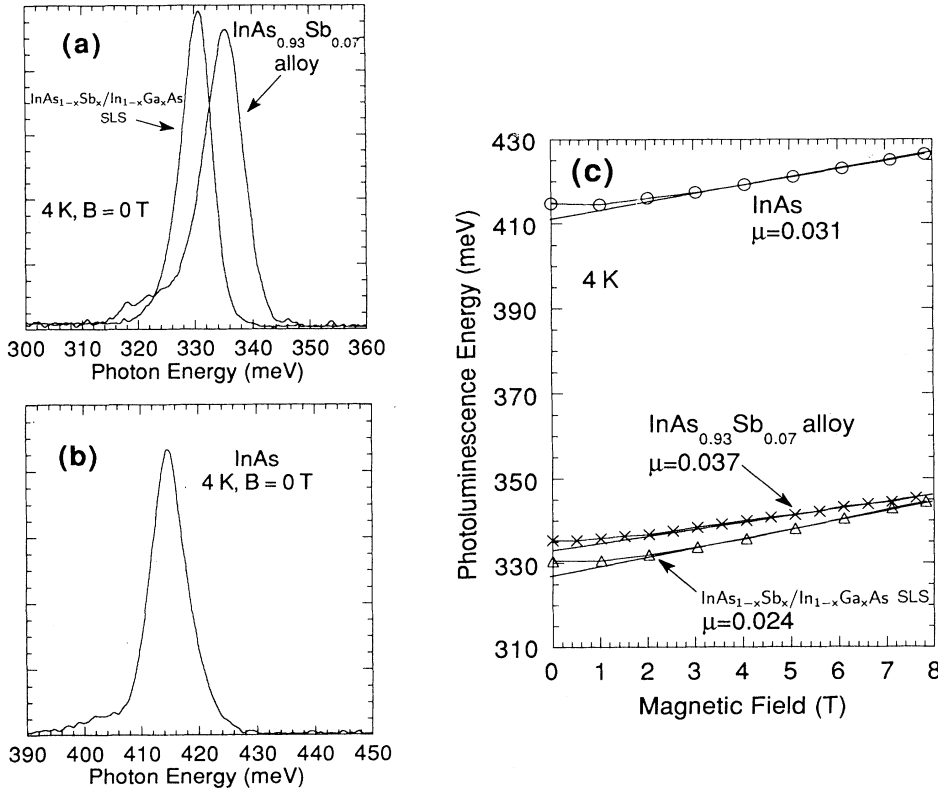


FIG. 1. Low-temperature photoluminescence spectra for the $\text{InAs}_{1-x}\text{Sb}_x/\text{In}_{1-x}\text{Ga}_x\text{As}$ SLS (a) and unstrained $\text{InAs}_{1-x}\text{Sb}_x$ (a) and InAs (b) alloys. The magnetic-field-induced shift of the photoluminescence energy is shown in (c), and reduced mass values (μ), corresponding to the slope, are indicated for each sample.

induced reduction in linewidth consistent with exciton scattering from ionized impurities.¹⁰ For $B > 2\text{T}$, the photoluminescence peak energies display a linear shift with the magnetic field. In the free electron-hole approximation, the field-induced shift for the lowest energy magnetoluminescence transition is described by

$$\frac{dE}{dB} = \frac{e\hbar}{2m_0c} \left[\frac{1}{m_e^*} + \frac{1}{m_h^*} \right] = \frac{e\hbar}{2m_0c\mu}, \quad (1)$$

where μ is the electron-hole-reduced effective mass. Reduced mass values for each sample, corresponding to the slope, are shown in Fig. 1(c). The reduced mass of the SLS was less than that of the alloys because the in-plane hole mass decreased significantly in the biaxially compressed $\text{InAs}_{1-x}\text{Sb}_x$ layers of the SLS.

Auger threshold energies are frequently observed through the temperature dependence of processes involving minority carrier lifetime. (For example, photoconductivity, p - n junction resistance, radiative efficiency, etc.) The temperature dependence of the photoluminescence intensity is shown in Fig. 2 for the SLS, $\text{InAs}_{0.93}\text{Sb}_{0.07}$, and InAs samples. In all samples, the radiative efficiency at low temperature is insensitive to temperature, probably due to nonradiative recombination at dislocations or impurities. At $>100\text{K}$, the radiative efficiency decreases exponentially; the approximate thermal activation energy (ΔE) for each sample is shown in Fig. 2. The activation energy of the SLS was significantly larger than that of the unstrained alloys ($\Delta E = 0.26E_{\text{gap}}$ vs $\Delta E = 0.06E_{\text{gap}}$). Other $\text{InAs}_{1-x}\text{Sb}_x/$

$\text{In}_{1-x}\text{Ga}_x\text{As}$ SLS's that we examined also displayed large activation energies. Due to variations in optical alignment and sample doping and defects, the differences in the relative radiative efficiency between samples may not be accurate.

Approaching room temperature, Auger-1 will be the dominant nonradiative process in extrinsic, n -type material. The radiative efficiency is

$$\eta = \frac{\tau_A}{\tau_R} \propto (1/n_0) \exp\left(\frac{\Delta E}{kT}\right), \quad (2)$$

$$\Delta E = \left[\frac{m_e^*/m_h^*}{1 + (m_e^*/m_h^*)} \right] E_{\text{gap}}, \quad (3)$$

where n_0 is the electron density, $\tau_R \propto (T/n_0)$ is the radiative lifetime, and $\tau_A \propto (T/n_0^2) \exp(\Delta E/kT)$ is the Auger-1 lifetime (in two dimensions).^{11,12} Due to the doping level in these samples, the intrinsic carrier concentration can be neglected at $<300\text{K}$. Equation (3) is based on simple energy-momentum conservation for isotropic, parabolic bands, and the activation energy, ΔE ($\Delta E = \text{Auger threshold} - \text{Band gap}$), is valid in two or three dimensions.¹¹ In the two-dimensional limit, the SLS in-plane effective masses determine ΔE ,^{2,3} and therefore, the SLS activation energy is larger than that of the unstrained alloys due to the decreased hole mass in biaxially compressed layers of the SLS.

In a superlattice, the Auger-1 process consists of transitions between subbands involving electron-hole recombination ($1e \rightarrow 1h$) and scattering of an energetic electron

($1e' \rightarrow Ne'$). (Assuming that only the lowest-energy subbands are populated.) When the energetic electron remains in the same subband ($N=1$), ΔE is large and Eq. (3) is valid.¹¹ For scattering processes to higher subbands ($N=2,3,\dots$), ΔE decreases.¹³ Consider the \hat{z} (growth direction) dependence of the Auger-1 matrix element,

$$M \propto G_{1e,1h} G_{1e',Ne'} \quad (4)$$

where $G_{jk} = \langle j | \exp(iqz) | k \rangle$ is a scattering integral. Using a tight-binding representation of the subbands, we write G_{jk} as

$$G_{jk} = \langle \Phi_j | e^{iqz} | \Phi_k \rangle \delta(q_j - q_k - q), \quad (5)$$

where $|\Phi_j\rangle$ is an isolated quantum-well, envelope function. In Eq. (5), the δ function conserves momentum (q) in the reduced Brillouin zone, and the matrix element depends on the Fourier components of the envelope functions. Using simple envelope functions to evaluate M , one finds that scattering to higher energy subbands decreases rapidly as $|q| \rightarrow 0$, and intersubband scattering is weak for roughly, $|q| < \pi/d_{1e}$, where d_{1e} is the effective width of the $|\Phi_{1e}\rangle$. In the reduced Brillouin zone, $|q| \leq 2\pi/d$, where d is the superlattice period. Therefore, for superlattices satisfying the rule, $d_{1e} < d/2$, scattering to higher subbands is suppressed, and ΔE approaches the two-dimensional value [Eq. (3)]. Summarizing the discussion, an increased Auger-1 threshold energy (or ΔE) should be observed in an SLS when (1) biaxial compression of the quantum well increases the effective-mass ratio (m_e^*/m_h^*), (2) the superlattice has thin wells and thick barriers such that ($d_{1e} < d/2$) is satisfied, and (3) subbands are separated in energy sufficiently to limit population of higher-energy subbands and to prevent an increase of the hole mass through the interaction with light-hole subbands.

A transfer-matrix calculation of the SLS band structure was performed using an 8×8 $\mathbf{k} \cdot \mathbf{p}$ Hamiltonian.¹⁴

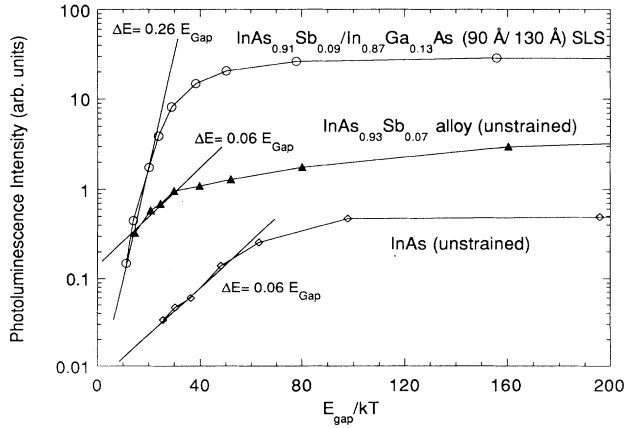


FIG. 2. Temperature dependence of the photoluminescence intensity (radiative efficiency) for the $\text{InAs}_{1-x}\text{Sb}_x/\text{In}_{1-x}\text{Ga}_x\text{As}$ SLS and $\text{InAs}_{1-x}\text{Sb}_x$ and InAs alloys. Activation energies (ΔE) corresponding to the exponential decrease in radiative efficiency at high temperature are indicated in the figure.

Except for ternary band-gap values, $\mathbf{k} \cdot \mathbf{p}$ parameters for InAs were used in the calculation.¹⁵ In the Hamiltonian, the conduction-band offset was estimated from quantum-size shifts observed in $\text{InAs}_{1-x}\text{Sb}_x$ SLS's and quantum wells, and the value of the anomalous, bulk $\text{InAs}_{0.91}\text{Sb}_{0.09}$ band gap was determined from the measured photoluminescence energy.¹⁶ The proposed SLS band structure is shown in Fig. 3. Overall, the SLS appears to conform to the guidelines for exhibiting increased Auger-1 threshold energy. The $1e$ subband is strongly confined ($d_{1e} \approx 110 \text{ \AA} = d/2$), and there is significant separation between the $1hh$ - $1lh$ and $1e$ - $2e$ states in energy. The interaction between the $1hh$ and $1lh$ states is weak, and the $1hh$ state has a low in-plane effective mass at band extrema, $0.029m_0$. The effective mass of the $1e$ electron is $0.016m_0$, resulting in $m_e^*/m_h^* = 0.55$. Using band extrema, effective-mass values obtained from the $\mathbf{k} \cdot \mathbf{p}$ calculation, $\Delta E = 0.35E_{\text{gap}}$ for the SLS in the two-dimensional limit. Nonparabolicity of the conduction-band, intersubband scattering, and band filling produce deviations in the Auger-1 threshold from this estimate.

From magneto-optical spectra, photoluminescence (PL) temperature dependence, and band-structure calculations, we estimated the in-plane effective mass ratio (m_e^*/m_h^*) for SLS and alloy samples (see Table I). Theoretical values were obtained from the literature values for InAs (Ref. 15) or from the $\mathbf{k} \cdot \mathbf{p}$ calculation for the SLS. Equation (3) was used to estimate the mass ratio from the measured values of ΔE . Assuming that the electron masses are the same in the SLS and the alloys, we used alloy and SLS reduced masses to estimate the

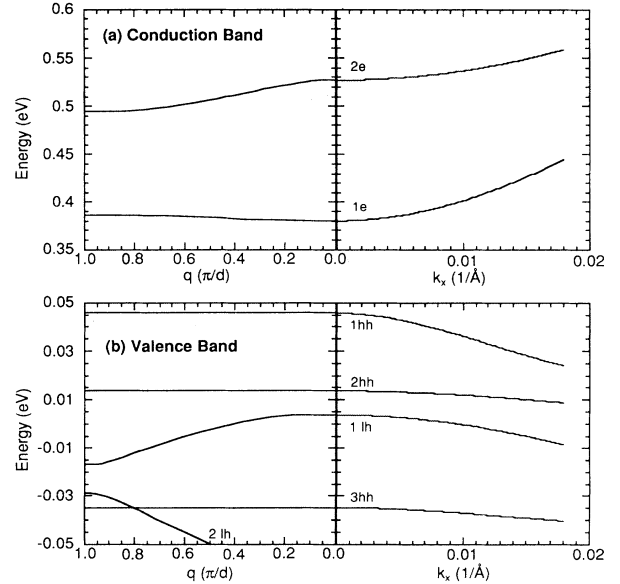


FIG. 3. Proposed band structure for the $\text{InAs}_{1-x}\text{Sb}_x/\text{In}_{1-x}\text{Ga}_x\text{As}$ SLS determined from a $\mathbf{k} \cdot \mathbf{p}$ calculation. Conduction-band (a) and valence-band (b) energies are shown for in-plane wave vector, k_x ($q=0$), and subband wave vector, q ($k_x=0$). The unstrained valence band of InAs is the reference point (energy=0). The SLS period, d , is 220 \AA .

TABLE I. Theoretical and experimentally determined effective-mass ratios (m_e^*/m_h^*) for the $\text{InAs}_{1-x}\text{Sb}_x/\text{In}_{1-x}\text{Ga}_x\text{As}$ SLS and unstrained $\text{InAs}_{1-x}\text{Sb}_x$ and InAs alloys.

| Sample | Theory (Ref. or $\mathbf{k}\cdot\mathbf{p}$) | PL vs T (Auger) activation energy) | Magnetooptical |
|--|---|---|----------------------|
| InAs | 0.06 | 0.06 | ($m_e^*=0.023m_0$) |
| $\text{InAs}_{0.93}\text{Sb}_{0.07}$ | 0.06 | 0.06 | ($m_e^*=0.026m_0$) |
| SLS | 0.55 | 0.35 | 0.3–0.5 |
| $\text{InAs}_{0.91}\text{Sb}_{0.09}/$ $\text{In}_{0.87}\text{Ga}_{0.13}\text{As}$ (90 Å/130 Å) | | | |

effective-mass ratio of the SLS [$m_e^*/m_h^*=(\mu_{\text{alloy}}/\mu_{\text{SLS}})-1$]. (In Table I, electron effective masses for the alloys were obtained by correcting the reduced masses for exciton binding and nonparabolicity effects.¹⁷) For each sample, theoretical and experimentally estimated mass ratios are in reasonable agreement, and comparing the SLS with the alloys, the SLS consistently displayed the predicted effects of the valence band under biaxial compression.

In conclusion, we have performed a comparative study of SLS's with biaxially compressed $\text{InAs}_{1-x}\text{Sb}_x$ and unstrained $\text{InAs}_{1-x}\text{Sb}_x$ alloys. The expected decrease of the in-plane hole mass for the SLS was observed in magnetophotoluminescence measurements. The photoluminescence efficiency versus temperature revealed that an increased activation energy for nonradiative recombination accompanies the decreased hole mass in the SLS's. Photoluminescence efficiency activation energies for the SLS and unstrained alloys are consistent with

band extrema estimates of Auger-1 threshold energies, with the activation energy for the SLS approaching the Auger-1 value in the two-dimensional limit. Guidelines are presented for designing heterostructures with increased Auger-1 threshold energies. We anticipate that long-wavelength diode lasers will be constructed, where an increased Auger-1 threshold energy is confirmed through characteristics of the device and higher temperature operation is demonstrated.

We thank E. D. Jones, S. K. Lyo, and H. P. Hjalmarson for useful discussions. D. M. Follstaedt performed electron microscope measurements on $\text{InAs}_{1-x}\text{Sb}_x$ samples. J. A. Bur, K. C. Baucom, and M. W. Pelczynski provided technical assistance. This work was performed at Sandia National Laboratories, supported by the U.S. Department of Energy under Contract No. DE-AC04-94AL85000.

- ¹S. J. Eglash and H. K. Choi, *Appl. Phys. Lett.* **57**, 1292 (1990); **61**, 1154 (1992).
²A. R. Adams, *Electron. Lett.* **22**, 249 (1986).
³E. Yablonovich and E. O. Kane, *IEEE J. Lightwave Technol.* **6**, 1292 (1988).
⁴C. H. Grein, P. M. Young, and H. Ehrenreich, *Appl. Phys. Lett.* **61**, 2905 (1992).
⁵S. R. Kurtz, R. B. Biefeld, L. R. Dawson, K. C. Baucom, and A. J. Howard, *Appl. Phys. Lett.* **64**, 812 (1994).
⁶H. K. Choi, G. W. Turner, and Z. L. Liao (unpublished).
⁷V. S. Speriosu, M. A. Nicolet, S. T. Picraux, and R. M. Biefeld, *Appl. Phys. Lett.* **45**, 223 (1984); M. Fatemi and R. E. Stahlbush, *ibid.* **58**, 825 (1991).
⁸Z. M. Fang, K. Y. Ma, D. H. Jaw, R. M. Cohen, and G. B. Stringfellow, *J. Appl. Phys.* **67**, 7034 (1990), and references therein.
⁹D. M. Follstaedt, R. M. Biefeld, S. R. Kurtz, and K. C. Baucom, *J. Electron. Mater.* (to be published).
¹⁰S. K. Lyo, E. D. Jones, and S. R. Kurtz, *J. Lumin.* **60&61**, 409 (1994).
¹¹N. K. Dutta, *J. Appl. Phys.* **54**, 1236 (1983); G. P. Agrawal and N. K. Dutta, *Long-Wavelength Semiconductor Lasers* (Van Nostrand Reinhold, New York, 1986).
¹²M. A. Kinch, M. J. Brau, and A. Simmons, *J. Appl. Phys.* **44**, 1649 (1973). The three-dimensional (3D) expressions for radiative and Auger lifetime are both proportional to $T^{3/2}$. The SLS will display an intermediate-temperature dependence be-

- tween the 2D and 3D expressions, and corrections to the temperature dependence of Eq. (2) are negligible.
¹³C. Smith, R. A. Abram, and M. G. Burt, *Superlatt. Microstruct.* **1**, 119 (1985).
¹⁴B. Chen, M. Lazzouni, and L. R. Ram-Mohan, *Phys. Rev. B* **45**, 1204 (1992); L. R. Ram-Mohan, K. H. Yoo, and R. L. Aggarwal, *ibid.* **38**, 6151 (1988).
¹⁵L. M. Kanskaya, S. I. Kokhanovskii, R. P. Seisyan, A. L. Efros, and V. A. Yukish, *Fiz. Tekh. Poluprovodn.* **17**, 718 (1983) [*Sov. Phys. Semicond.* **17**, 449 (1983)].
¹⁶S. R. Kurtz and R. M. Biefeld, *Appl. Phys. Lett.* **66**, 364 (1995).
¹⁷Assuming an infinite hole mass in the unstrained alloys, Eq. (1) can be rewritten as

$$\frac{dE}{dB} \approx \frac{\mu_B}{m_e^*} \left[1 - \frac{1.6}{3} \left[\frac{m_e^* R}{\mu_B B} \right]^{2/3} - \frac{2\mu_B \kappa B}{m_e^* E_{\text{gap}}} \right],$$

where μ_B is the Bohr magneton. InAs values were used to evaluate this expression. The middle term is a correction for exciton binding [$R=1.8$ meV, see E. A. Johnson, *Semiconductors and Semimetals*, edited by R. K. Willardson and A. C. Beer (Academic, New York, 1967), Vol. 3, p. 228] and the last term is a correction for the nonparabolicity of the conduction band [$\kappa=1.6$, G. M. Sundaram *et al.*, *Semicond. Sci. Technol.* **7**, 985 (1992)]. The larger electron effective mass observed in the $\text{InAs}_{0.93}\text{Sb}_{0.07}$ alloy may be caused, in part, by ordering of the alloy.